Localizing Exciton Recombination Sites in Conformationally Distinct Single Conjugated Polymers by Super-resolution Fluorescence Imaging

Heungman Park,[†,#] Dat Tien Hoang,[†,#] Keewook Paeng,[†,‡] and Laura J. Kaufman[*,†]

[†]Department of Chemistry, Columbia University, New York, New York 10027, United States and [‡]Department of Chemistry, Sungkyunkwan University, Suwon 440-746, Republic of Korea. [#]These two authors (H.P. and D.T.H.) contributed equally to this work.

ABSTRACT To thoroughly elucidate how molecular conformation and photophysical properties of conjugated polymers (CPs) are related requires simultaneous probing of both. Previous efforts used fluorescence imaging with one nanometer accuracy (FIONA) to image CPs, which allowed simultaneous estimation of molecular conformation and probing of fluorescence intensity decay. We show that calculating the molecular radius of gyration for putative folded and unfolded poly(2-methoxy-5-(2′-ethylhexyloxy)1,4-phenylenevinylene) (MEH-PPV) molecules using FIONA underestimates molecular extension by averaging over emitters during localization. In contrast, employing algorithms based on single molecule high resolution imaging with photobleaching (SHRImP), including an approach we term all-frames SHRImP, allows localization of individual emitters. SHRImP processing corroborates that compact MEH-PPV molecules have distinct photophysical properties from extended ones. Estimated radii of gyration for isolated 168 kDa MEH-PPV molecules immobilized in polystyrene and exhibiting either stepwise or continuous intensity decays are found to be 12.6 and 25.3 nm, respectively, while the distance between exciton recombination sites is estimated to be ∼10 nm independent of molecular conformation.

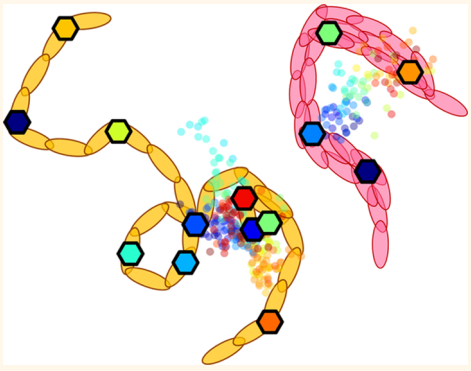

KEYWORDS: conjugated polymer · MEH-PPV · exciton recombination · emission site localization · fluorescence imaging · super-resolution microscopy · FIONA · SHRImP

Conjugated polymers (CPs) have gained attention as possible materials for next-generation electronic and electro-optical devices. Unfortunately, analysis and control of CP properties are often complicated by polydispersity, morphological diversity, and chemical and physical defects. Understanding how these properties affect CP photophysics on a single molecule level is an important step in understanding how such photophysics could be controlled in more complex environments such as thin films, where both intra- and intermolecular CP contacts are present.

Single molecule studies on isolated CPs have measured fluorescence polarization anisotropy and polarization modulation depth.[1−7] While such measurements provide information about average CP conformation (especially when coupled with simulation), they do not allow simultaneous recording of CP fluorescence intensity transients. Photophysical behavior of a CP is expected to be highly dependent on its conformation and can be characterized in part by following its fluorescence intensity in time. For example, across-chain exciton migration is expected to lead to few emitters and stepwise photobleaching while the less efficient along-chain exciton migration would result in many emitters and continuous photobleaching behavior.[8−12] These behaviors are, in turn, believed to be characteristic of folded and unfolded CP conformations.[4,8−13] To validate this hypothesis, simultaneous measurement of fluorescence intensity transients and extraction of conformation of single CPs is required.

Super-resolution imaging approaches could be used to simultaneously assess molecular conformation and photophysics of

* Address correspondence to kaufman@chem.columbia.edu.

Received for review January 6, 2015 and accepted March 5, 2015.

Published online 10.1021/acsnano.5b00086

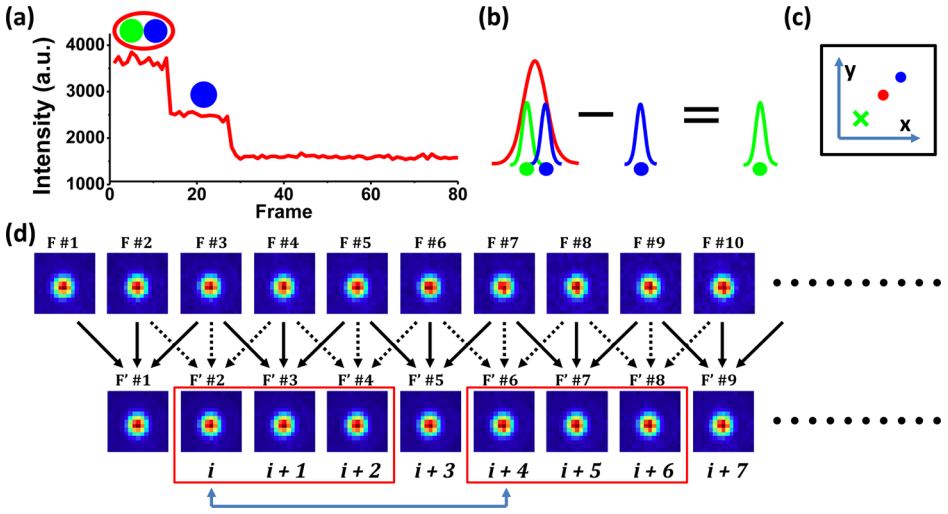

Figure 1. (a) An intensity trajectory with two emission sites (indicted by blue and green dots) that photobleach serially. (b) Schematic depiction of SHRImP analysis: The final emitter (blue) is localized *via* FIONA, and the position of each earlier emitter (in this depiction, there is a single such emitter, depicted in green) is found *via* localization after SHRImP image subtraction. If only FIONA is employed, when multiple emitters are present, the determined position (red) will represent an average over all emission sites. (c) Schematic depiction of localized positions as determined by FIONA (red and blue dots) and SHRImP (green cross). (d) Particular SHRImP implementation employed in this work. Each frame image, F, is averaged with adjacent images to produce a second set of frames, F′, to mitigate noise. SHRImP is calculated for frame (F′) *i* with frames (F′) of $(i+n)_{n=3,4,5,6}$. If frame pair $\{i, i+4\}$ satisfies the fit uncertainty and eccentricity constraints described in the text, all SHRImP combinations for frames depicted in the two red boxes are calculated. The frame pair yielding the minimum fit uncertainty is used to determine the position of an emission site.

conjugated polymers since such approaches can provide subdiffraction limit spatial resolution of multiple emission sites within the diffraction limit and, provided that the appropriate technique is used, allow for time-dependent intensity measurement as well.[14−19] Fluorescence imaging with one-nanometer accuracy (FIONA) has previously been used to precisely identify the centroid position of emission from single CPs.[18,19] By mapping the centroid position over time using FIONA, molecular conformations of single CPs were traced out. In certain cases, CP conformation was found to be quite extended, and on such molecules sudden jumps in the centroid position were seen. These jumps were often correlated with stepwise transitions in the fluorescence intensity transients.[19] This correlation suggested that shifts of the centroid were the result of changes in number and/or position of emitting site(s).

While these experiments were the first to directly probe molecular conformation while tracking fluorescence intensity, FIONA cannot provide quantitative characterization of a CP's conformation if that CP has multiple simultaneously emitting sites. In this case, the centroid localized through FIONA will report the average position of all such emitting chromophores, with this position weighted by the fluorescence intensity of each emitter. The failure of FIONA to trace out molecular conformation will be exacerbated for molecules with a large number of emitters (as is expected on CPs with extended conformation). To avoid the averaging inherent in FIONA for CPs with multiple simultaneous emitters, single molecule high resolution imaging with photobleaching (SHRImP)[16,17,20] or the equivalent techniques of nanometer localized multiple single molecule (NALMS)[21] and bleaching/blinking assisted localization microscopy (BaLM)[22] can be employed. These techniques rely on the stochastic nature of photobleaching and image subtraction to resolve individual emitters within a diffraction-limited spot and thus can be used to spatially resolve individual emitters along a CP experiencing serial emitter photobleaching. A schematic diagram illustrating the SHRImP procedure is shown in Figure 1a−c.

In this paper, we use a SHRImP algorithm to map out the positions of individual emitters along single poly(2-methoxy-5-(2′-ethylhexyloxy)1,4-phenylenevinylene) (MEH-PPV) molecules exhibiting monotonically decreasing intensity, likely due to serial photobleaching. We also develop a variant of this technique, all-frames SHRImP (afSHRImP), in which all possible image subtractions are performed combinatorially to reduce uncertainty associated with localized emission sites. Using SHRImP and afSHRImP, we estimate the radius of gyration projected onto the sample plane of single MEH-PPV chains immobilized in polystyrene and corroborate correlation between photobleaching behavior and CP conformation.

DATA ANALYSIS

All movies were assessed using both frame-by-frame FIONA and SHRImP. Both types of analyses were performed on movies whose adjacent frames (F) were averaged, resulting in a movie in which each frame (F′) is an average of three images (Figure 1d). This averaging was performed to mitigate the anticipated noise

increase when subtracting images during SHRImP analysis.

Both FIONA and SHRImP analysis require 2D-Gaussian fitting of images. The general 2-D Gaussian function is given by

$$I(x, y) = Ae^{-\{B(x - x_0)^2 + C(x - x_0)(y - y_0) + D(y - y_0)^2\}} + I_0 \quad (1)$$

for which average fit uncertainty and eccentricity are calculated as $\delta r = {}^1/_2(\delta x + \delta y)$ and $e = (1 - (l^2/L^2))^{1/2}$, where L is the semimajor axis and l is the semiminor axis of the fitted Gaussian. In FIONA, localization accuracy as obtained from various experimental parameters[14] is quite similar to that obtained using Gaussian fit uncertainty as suggested by Selvin *et al.*,[17] and we use that measure of fit uncertainty in this study. In an ideal situation, the 2D Gaussian fit of the centroid associated with a single emitter would have an eccentricity of 0. However, in experiments the fits may not be perfectly symmetric not only because the MEH-PPV molecules may consist of multiple emission sites but also because the images include noise from a variety of sources, and distortions occur due to pixelation, imperfect optical alignment, and orientation effects.[14,23,24] We demonstrated that eccentricity is nonzero for single emitters by performing FIONA on single PDI dye molecules (pPDI: *N,N′*-bis(3-phosphonopropyl)-3,4,9,10-perylene dicarboximide) and 3.5 nm diameter CdSe−ZnS core−shell quantum dots, both of which are considered single point-source emitters. In both cases, 2D Gaussian fit eccentricities typically ranged from 0.4 to 0.6. Such eccentricities were also seen for MEH-PPV molecules with multiple single emitters within the diffraction limit. At a typical signal-to-background ratio (SBR) for MEH-PPV molecules in this experiment (SBR $\approx$ 1.4−2.1), fit uncertainty is approximately 0.07 pixels (~7 nm). The subtracted images produced for SHRImP analysis have increased uncertainty due to error propagation, with $(2)^{1/2}\delta r \approx 0.10$ pixels.

Following frame averaging and frame-by-frame FIONA analysis, SHRImP analysis was then used to localize individual emitters along MEH-PPV molecules as shown schematically in Figure 1. Images obtained from frame subtractions were retained if the resulting image was fit to a 2D Gaussian with (1) fit uncertainty $\leq$ 0.10 pixels and (2) eccentricity $\leq$ 0.55. These values were set empirically and may differ for experimental conditions yielding different SBR. While the original SHRImP algorithm interrogated only time-adjacent frames,[16,17] the presence of stochastic noise results in particular frames having poorer than average signal-to-noise, which in turn would lead to poorer than average images generated through SHRImP subtractions using such frames. As such, the SHRImP algorithm was modified to include not only frame pairs that are time-adjacent but also those in the local time vicinity, as shown schematically in Figure 1 and explored in an example described here. A subtracted image for a pair of frames, $\{i, i+3\}$, is calculated, and its Gaussian fit eccentricity and uncertainty are compared with the constraints. If the frame pair does not satisfy the constraints, SHRImP of the next pair, $\{i, i+4\}$, is calculated. The same procedure is repeated until the pair $\{i, i+6\}$ is reached. Because frames $i+1$ and $i+2$ have constituents in common with frame i, the pairs $\{i, i+1\}$ and $\{i, i+2\}$ are not included in the SHRImP analysis. If analysis of the last pair within the range defined does not satisfy the constraints, no SHRImP fits are retained for frame i, and the algorithm is repeated for frame $i+1$. If any pair of frames $\{i, i+n\}_{n=3,4,5,6}$ does yield an image that satisfies the fit constraints, all combinations $\{i, j\}$ with $i = i, i+1, i+2$, and $j = j, j+1, j+2$ are assessed. If multiple pairs for this frame combination satisfy the constraints, the combination whose result has minimum fit uncertainty is chosen.

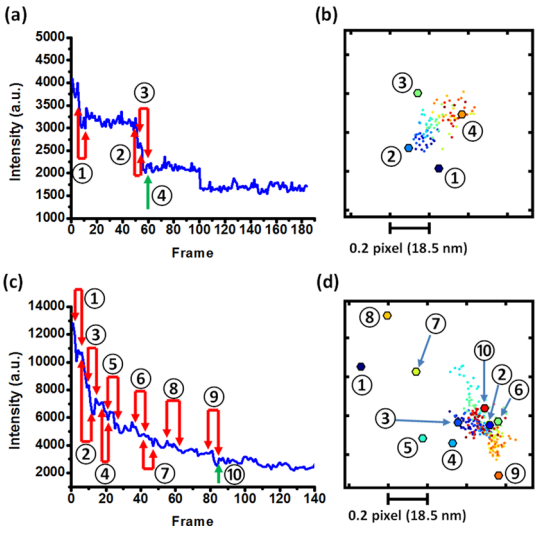

Figure 2. Intensity trajectory of MEH-PPV polymers with (a) stepwise and (c) continuous intensity decays. Red arrows indicate frame pairs found by the SHRImP data analysis algorithm depicted in Figure 1, and the single green arrow indicates the frame from which the final emitter is localized by FIONA. (b,d) Large dots are emission sites localized from the frames indicated by red and green arrows in panels a and c. Small dots indicate frame-by-frame FIONA centroid localization for these molecules. Colors correspond to the order of pairs and order of frames from navy to red for both SHRImP and frame-by-frame FIONA, with color changes in FIONA set by initial position of frame pairs identified *via* SHRImP. Each tick in panels b and d corresponds to 0.2 pixel separation with 92.5 nm/pixel magnification. The RMS distances for these MEH-PPV molecules are found to be 17.0 ± 13.4 nm and 30.1 ± 21.9 nm *via* SHRImP analysis for the molecules depicted by panels b and d, respectively.

RESULTS

A. Example Stepwise and Continuous Trajectories. Figure 2 illustrates the SHRImP approach depicted schematically in Figure 1 for two example molecules, one with stepwise photobleaching and one with continuous photobleaching. For the molecule depicted in Figure 2a,b, the first frame pair identified by the

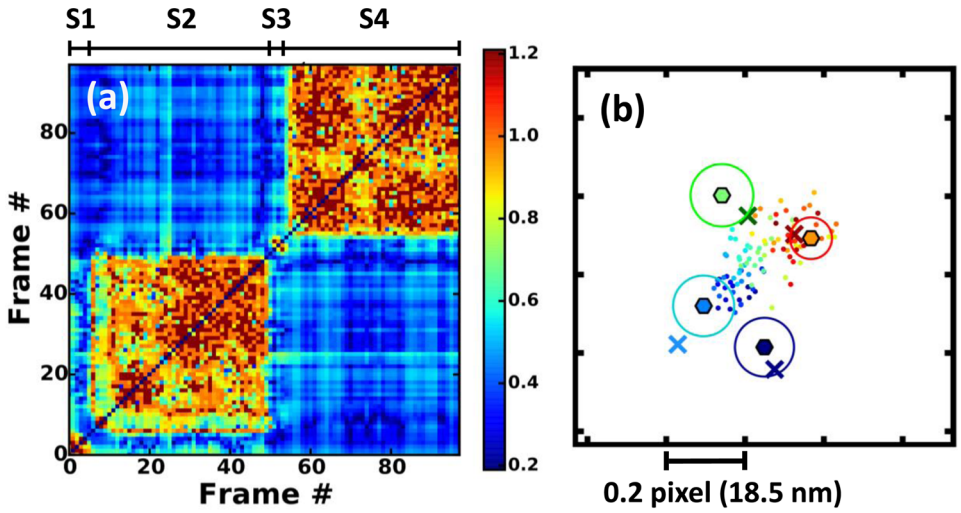

Figure 3. (a) Two dimensional contour plot of frame-to-frame eccentricity of SHRImP fits for the molecule depicted in Figure 2a,b. If the algorithm could not fit a SHRImP image, $e = 1.2$ was assigned (dark brown color). Frames are assigned to sections S1−S4 by grouping sections of poor SHRImP fits, indicated by yellow-brown colors on the plot. (b) afSHRImP localization of emitters on the molecule depicted in Figure 2a,b. Crosses are emission sites localized by afSHRImP as described in the text and shown in Supporting Information, Figure S3. Error bars are smaller than the symbol size. Large hexagonal symbols are emission sites identified by a standard implementation of SHRImP as also shown in Figure 2b, with fit uncertainty represented by the outer circles. The first emitter is shown in navy, the second in blue, the third in green, and the fourth in red. Small dots are frame-by-frame FIONA localizations with colors corresponding to the order of frames from navy to red. Each tick in panel b corresponds to 0.2 pixel separation with 92.5 nm/pixel magnification.

SHRImP algorithm described above that satisfies the constraints is frame pair {3,8}. All combinations of frames 3,4,5 with frames 8,9,10 are then assessed, and frame pair {5,10} is chosen because it has the minimum fit uncertainty of the tested pairs. The fit results from that frame pair determine the position of the first emission site, denoted ① in Figure 2b. Images from this frame pair as well as the SHRImP subtracted image and associated fits are shown in Supporting Information, Figure S1. Using the same approach, the remaining emission sites are determined. We note that the last emission site, ④ in Figure 2b, is determined by performing FIONA on the final frame identified *via* SHRImP analysis, as FIONA and SHRImP will return the same result in the presence of a single emitter, and FIONA localization avoids the noise introduced by SHRImP subtraction. In Figure 2a, the paired red arrows indicate the frame pairs identified by the SHRImP data analysis process, and the single green arrow indicates the frame used for FIONA localization of the final emitter. For the molecule depicted in Figure 2a,b, a total of four emission sites were identified. These emission sites are plotted in Figure 2b as large dots. FIONA localizations for every frame of the averaged movie are shown with small dots for comparison. The root-mean-squared (RMS) distance, $({}^1/_N \Sigma_i^N |\vec{r}_i - \vec{r}_{ave}|^2)^{1/2}$, of the four emission sites identified *via* SHRImP was found to be 17.0 ± 13.4 nm. Because each SHRImP fit has 5−7 nm uncertainty, the RMS distance uncertainty is relatively large.

The same SHRImP analysis can also be used to identify emitter locations along molecules with continuous photobleaching behavior, as shown for an example molecule in Figure 2c,d. Even though such molecules reveal few abrupt changes in intensity, the SHRImP algorithm identifies pairs of frames that, when subtracted, yield images that are well fit and meet the constraints described above. In this molecule, 10 emitters are found (with RMS distance of 30.1 ± 21.9 nm), as shown in Figure 2d.

B. Enhanced Precision of Localization of Emission Sites. Employing SHRImP as described above results in relatively high uncertainty in localization of individual emitters. This is primarily caused by noise that is exacerbated when performing subtractions between frames. In cases where intensity trajectories are stepwise, where undercounting of emitters is not expected, error in localizing emitters can be minimized by statistical averaging through a variant of SHRImP we call all-frames SHRImP (afSHRImP).

Here, every pair of frames (F′) in a trajectory is subject to SHRImP subtraction. The 2D Gaussian fits from the resulting images are visualized by plotting their eccentricities in a matrix, as shown in Figure 3a for the molecule depicted in Figure 2a,b. Low eccentricity areas (depicted in blue and cyan) indicate that the corresponding frame pairs have good SHRImP fits. For example, frame pair {20, 40} has a bad SHRImP fit ($e \approx 0.9$, orange) while frame pair {20, 60} has a good SHRImP fit ($e \approx 0.4$, blue). Similar 2D matrix plots can be made for fit uncertainties (Supporting Information, Figure S2); frames {20,40} and {20,60} have SHRImP fits with uncertainties of ~200 and 3.9 nm, respectively.

After generating the eccentricity contour map, rather than only considering fit results for adjacent and near-adjacent frames as depicted in Figure 1,

trajectories are divided into and inspected by sections. Visual inspection of the contour map reveals color correlations over sets of frames. For example, all combinations of frames 1−6 yield SHRImP subtractions with poor fits (as shown through high eccentricity in Figure 3a), suggesting that no change in emitter number or position has occurred during this period. This set of frames is then considered a section and denoted S1 in Figure 3a. For frames in S1, an abrupt and persistent color transition to blue in the eccentricity contour map is seen when SHRImP subtractions are performed between frames in this section and frames 7 and higher, indicating that a change in emitter number and/or position has occurred. From visual inspection of square regions with concentrated yellow−dark brown colors, the trajectory is separated into four sections (S1, S2, S3, and S4 in Figure 3a) for analysis that allows more precise determination of emitter position than does the SHRImP algorithm already described.

In afSHRImP, the first photobleached emission site is determined by averaging the identified positions of every SHRImP calculation between frames in sections 1 and 2 weighted by their fit uncertainties, and this procedure is repeated for determination of each emission site (Supporting Information, Figure S3). The emission sites localized by afSHRImP for the molecule depicted in Figure 2a,b are shown in Figure 3b with crosses. For comparison, the emission sites identified through the implementation of SHRImP depicted in Figure 1 and shown in Figure 2b are also shown, with outer circles representing uncertainty in position.

Following the afSHRImP procedure, the calculated RMS distance for the molecule depicted in Figure 2a,b is 18.7 ± 1.7 nm. This is within the uncertainty of the RMS estimation of 17.0 ± 13.4 from a standard SHRImP implementation (Figure 2b). Performing this comparison on several molecules with stepwise photobleaching trajectories chosen at random reveals that the two SHRImP-based approaches yield quantitatively different RMS values, but in all cases the RMS value obtained *via* afSHRImP is within the uncertainty of that obtained by standard SHRImP analysis (Table 1), thus validating that approach. Given the similarity between SHRImP and afSHRImP results and because afSHRImP is appropriate for stepwise trajectories only, standard SHRImP is used in the analysis described below.

C. Correlation between MEH-PPV Photophysics and Conformation. The single chain properties of MEH-PPV are very challenging to ascertain from typical experiments given the molecules' tendency to aggregate.[25,26] In single molecule studies, MEH-PPV has been seen to assume various conformations in response to its interactions with both its host and solvent.[8−12,27] It has been inferred from polarization modulation depth measurements that when spin-coated from a solution of chloroform into a host polymer matrix, MEH-PPV preferentially adopts a stretched conformation while spin-coating from a solution of toluene leads to preference for a highly ordered, folded conformation.[9] We prepared samples by dissolving MEH-PPV in either toluene or chloroform before spin-coating into a polystyrene matrix. While both types of samples contained MEH-PPV molecules demonstrating both stepwise and continuously decaying intensity trajectories, the proportion of trajectories with stepwise bleaching was high in samples in which toluene was the solvent (for example, Figure 2a,b) while continuous bleaching trajectories were prevalent when chloroform was used (for example, Figure 2c,d). As described above, stepwise photobleaching is believed to indicate effective exciton funneling to a few recombination sites as can occur across chains, as would be facilitated through folded conformations. On the other hand, trajectories with higher initial and continuously decreasing intensities are indicative of the presence of many individual emission sites isolated along an extended molecule.[8−12] While intuitively an MEH-PPV molecule in a folded configuration will be more compact than one in a stretched conformation, to the best of our knowledge the actual size distributions of MEH-PPV molecules exhibiting stepwise and continuous photobleaching have not been reported previously. We estimated the size of MEH-PPV molecules demonstrating stepwise photobleaching (prepared from dissolution in toluene) and those with continuous photobleaching (prepared from dissolution in chloroform) projected onto the two-dimensional sample plane using SHRImP implemented as depicted in Figure 1 and compared those with estimated sizes as obtained *via* frame-by-frame FIONA.

RMS distances of the emission sites were calculated for 60 (toluene) and 61 (chloroform) MEH-PPV molecules displaying stepwise and continuous intensity decays as obtained from FIONA and SHRImP (Figure 4). If the emission sites are randomly distributed along the MEH-PPV chains, the RMS values are approximately equal to the radius of gyration of the polymers. FIONA yields median RMS distances of 8.2 and 11.9 nm for the stepwise and continuously photobleaching trajectories,

TABLE 1. Examples of RMS Distance and Associated Fit Uncertainty for Stepwise Photobleaching MEH-PPV Molecules by Standard SHRImP and afSHRImP

	standard SHRImP		afSHRImP	
no.	RMS (nm)	uncertainty (nm)	RMS (nm)	uncertainty (nm)
1	17.0	13.4	18.7	1.7
2	16.6	10.3	12.4	6.2
3	11.7	7.7	14.7	1.0
4	15.5	12.2	13.0	4.9
5	10.7	9.4	11.3	1.3
6	24.2	17.0	13.6	1.8
7	14.7	13.5	9.5	0.6

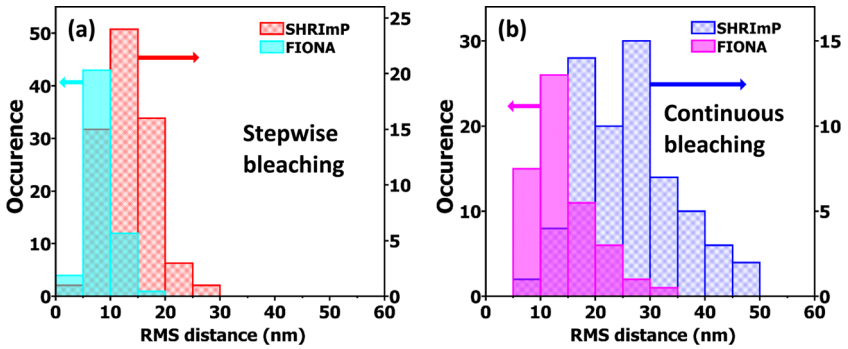

Figure 4. RMS distance histograms of emission sites identified by SHRImP and frame-by-frame FIONA for (a) 60 molecules with stepwise and (b) 61 molecules with continuous photobleaching intensity trajectories. Median RMS distances obtained are 8.2 (FIONA) and 12.6 (SHRImP) nm for molecules with stepwise bleaching trajectories and 11.9 (FIONA) and 25.3 (SHRImP) nm for molecules with continuously bleaching intensity trajectories.

respectively, suggesting that stepwise trajectories are associated with more compact conformations than continuously bleaching ones. This correlation is made more obvious through SHRImP analysis, where the median RMS distances obtained are 12.6 and 25.3 nm for molecules with stepwise and continuous intensity trajectories, respectively. Though each RMS value obtained *via* SHRImP has large relative uncertainty (~10 nm), there is a distinct difference in the peak values of the histograms associated with stepwise and continuously photobleaching molecules. For stepwise trajectories, we also assessed the radius of gyration using afSHRImP. As suggested by Table 1, because the differences in RMS distance as obtained by standard and afSHRImP are random and within a range near localization accuracy, there is no significant change in size distribution relative to that shown in Figure 4a when using afSHRImP (Supporting Information, Figure S4).

The ratio of median RMS distance obtained *via* SHRImP relative to FIONA, R_r, is 2.1 for continuously photobleaching trajectories and 1.5 for stepwise ones. The relatively large value of R_r for continuously photobleaching molecules is consistent with these molecules having many simultaneously emitting chromophores that FIONA averages over, thus yielding smaller observed positional changes with the photobleaching of a given emitter relative to SHRImP.

Typically 4−6 emission sites were found *via* SHRImP analysis for stepwise trajectories while 6−12 were found for continuously photobleaching trajectories. To assess whether the RMS distance distributions depend on the number of emission sites, the first five emission sites of MEH-PPV data shown in Figure 4b were used to recalculate the RMS distance distribution for molecules exhibiting continuous photobleaching. For example, the emission sites from ① to ⑤ in Figure 2c,d were used. The result showed that there is no significant difference between the two histograms with all emission sites and the first five emission sites (Supporting Information, Figure S5). This implies that the emission sites are distributed randomly in space and bleach randomly in time. We note that while SHRImP is expected to yield better estimates of number and position of emitters than can be achieved *via* FIONA, for continuously photobleaching trajectories there is likely an under-counting of emitters and residual averaging over multiple emitters. The fact that the RMS distance is not strongly affected by the number of emitters found in the range investigated suggests this does not prevent accurate estimation of molecular extension. Moreover, the fact that the identified emitters on molecules with continuous photobleaching trajectories are distributed widely in space argues against serious undercounting and residual averaging *via* SHRImP, as in this case a much tighter distribution of emitter positions would be expected.

The average RMS distances obtained *via* SHRImP are reasonable given that the end-to-end distance of the stretched M_w = 168k MEH-PPV molecules used here is ~417 nm (RMS distance ≈ 120 nm). To estimate the radius of gyration (R_g) of MEH-PPV, a semiflexible polymer, the worm-like chain (WLC) model may be employed. Here, if $L_c \gg L_p$,

$$R_g \approx \sqrt{\frac{1}{3} L_p L_c \left(1 - \frac{3L_p}{L_c}\right)} \qquad (2)$$

where L_c is the stretched length of the polymer and L_p is persistence length.[28] L_c is estimated by bN, where b is the length of the monomer and N is the number of monomers. We assign b as 0.6455 nm as assessed from the molecular structure (Supporting Information, Figure S6), and N is 646 for MEH-PPV molecules with M_w = 168 kDa. For MEH-PPV, L_p has been approximated as 6.51 and 7.33 nm for toluene and chloroform, respectively.[29] The resulting R_g values for the MEH-PPV used in this study are then 26.0 nm (toluene) and 27.5 nm (chloroform). The WLC model thus predicts R_g very similar to that measured for the continuously photobleaching MEH-PPV molecules assessed here (prepared from dissolution in chloroform) but suggests no significant difference for the radii of gyration of

MEH-PPV prepared from dissolution in toluene and chloroform. This contradicts most single molecule experimental data that do suggest conformation dependence on the solvent. The discrepancy may arise from solvent-dependent tension when MEH-PPV is immobilized in a host matrix during spin coating and/or particular ternary interactions between the conjugated polymer, solvent, and host matrix.[30,31] More rigorous theoretical models must be developed for accurate inclusion of such effects.

In addition to comparing the radius of gyration of the MEH-PPV molecules with stepwise and continuous photobleaching, the data collected allows determination of distance between nearest emitters. Our analysis is predicated on the presence of multiple simultaneous emitters, as is consistent with the monotonically decaying intensity trajectories analyzed. In this model, assessing distance between nearest identified emitters provides a measure of the exciton migration distance. We find that the median values of the nearest distance between emitters are 9.5 and 11.2 nm for stepwise and continuous trajectories, respectively (Supporting Information, Figure S7). The median exciton migration distance would be approximately half this distance or ~5 nm independent of conformation. This is consistent with previous findings that average exciton migration distance is less than or similar to 10 nm in MEH-PPV.[18,19,32]

CONCLUSIONS

It has previously been inferred that conjugated polymers exhibiting stepwise photobleaching are in folded conformations while those exhibiting continuously photobleaching trajectories are extended. We have prepared and investigated a set of molecules with stepwise and continuous photobleaching behavior and identify emitter positions through single molecule imaging and the super-resolution approach of SHRImP, as well as a variant termed afSHRImP that reduces the uncertainty associated with emitter localization. Using SHRImP rather than the localization microscopy approach of FIONA allows identification of emitter positions in both stepwise and continuous photobleaching trajectories and yields larger estimates of the molecular radius of gyration in reasonable agreement with theoretical predictions. We find molecules with stepwise trajectories are more compact than those with continuous photobleaching, consistent with previous suggestions. We demonstrate the utility of SHRImP for identifying emitter positions and corroborating the correlation between stepwise (continuous) photobleaching and compact (extended) conformation, estimate the radius of gyration of compact and extended MEH-PPV molecules (M_w = 168 kDa) as 12.6 and 25.3 nm, respectively, and provide an estimate of ~10 nm for the distance between recombination sites.

METHODS

MEH-PPV was synthesized following a previously described protocol.[33] The resultant MEH-PPV had M_w = 168 kDa with PDI = 2.1 with a single-peak trace on a gel-permeation chromatograph. For single-molecule measurements, MEH-PPV was diluted in ~4 wt % polystyrene (PS, Polymer Source, M_w = 6.4 kDa, PDI = 1.05) with toluene or chloroform as the solvent. These solutions were spin-coated at 2000 rpm onto glass slides resulting in ~200 nm thick films as measured *via* atomic force microscopy. The concentration of MEH-PPV in the solutions was $\sim 10^{-11}$ M to ensure that the average separation between CPs in the prepared film was greater than 1 μm. Experiments were performed on a home-built microscope in epi-fluorescence configuration with 532 nm wavelength excitation. An oil objective lens (60×, NA = 1.45) and additional magnification of ~1.5× resulted in a pixel size of 92.5 nm/pixel. The sample was illuminated with a power density of ~160 W/cm^2, and images were collected at a frame rate of 0.2 s on an EMCCD camera (Andor iXon DV-855). Resultant movies were analyzed using routines written in IDL and Python, the details of which are described in the main text. Because it is not trivial to correct sample drift in SHRImP analysis, only movies with drift below localization accuracy were subjected to further analysis. Drift assessment and correction is discussed in the Supporting Information.

Conflict of Interest: The authors declare no competing financial interest.

Supporting Information Available: Method for drift assessment and corrections; nine figures. This material is available free of charge *via* the Internet at http://pubs.acs.org.

Acknowledgment. This work was supported in part by the National Science Foundation under CHE 1213242 and a GRF for D.T.H. and in part by the Center for Re-Defining Photovoltaic Efficiency Through Molecule Scale Control, an Energy Frontier Research Center funded by the U.S. Department of Energy, Office of Science, Office of Basic Energy Sciences under DE-SC0001085.

REFERENCES AND NOTES

1. Thomsson, D.; Lin, H.; Scheblykin, I. G. Correlation Analysis of Fluorescence Intensity and Fluorescence Anisotropy Fluctuations in Single-Molecule Spectroscopy of Conjugated Polymers. *ChemPhysChem* **2010**, *11*, 897–904.
2. Lin, H.; Tabaei, S. R.; Thomsson, D.; Mirzov, O.; Larsson, P.-O.; Scheblykin, I. G. Fluorescence Blinking, Exciton Dynamics, and Energy Transfer Domains in Single Conjugated Polymer Chains. *J. Am. Chem. Soc.* **2008**, *130*, 7042–7051.
3. Furumaki, S.; Habuchi, S.; Vacha, M. Fluorescence-Detected Three-Dimensional Linear Dichroism: A Method to Determine Absorption Anisotropy in Single Sub-Wavelength Size Nanoparticles. *Chem. Phys. Lett.* **2010**, *487*, 312–314.
4. Kobayashi, H.; Onda, S.; Furumaki, S.; Habuchi, S.; Vacha, M. A Single-Molecule Approach to Conformation and Photophysics of Conjugated Polymers. *Chem. Phys. Lett.* **2012**, *528*, 1–6.
5. Bounos, G.; Ghosh, S.; Lee, A. K.; Plunkett, K. N.; DuBay, K. H.; Bolinger, J. C.; Zhang, R.; Friesner, R. A.; Nuckolls, C.; Reichman, D. R.; *et al.* Controlling Chain Conformation in Conjugated Polymers Using Defect Inclusion Strategies. *J. Am. Chem. Soc.* **2011**, *133*, 10155–10160.
6. Traub, M. C.; Lakhwani, G.; Bolinger, J. C.; Bout, D. V.; Barbara, P. F. Electronic Energy Transfer in Highly Aligned MEH-PPV Single Chains. *J. Phys. Chem. B* **2011**, *115*, 9941–9947.
7. Adachi, T.; Brazard, J.; Chokshi, P.; Bolinger, J. C.; Ganesan, V.; Barbara, P. F. Highly Ordered Single Conjugated Polymer

Chain Rod Morphologies. *J. Phys. Chem. C* **2010**, *114*, 20896–20902.
8. Huser, T.; Yan, M.; Rothberg, L. J. Single Chain Spectroscopy of Conformational Dependence of Conjugated Polymer Photophysics. *Proc. Natl. Acad. Sci. U.S.A.* **2000**, *97*, 11187–11191.
9. Sarzi Sartori, S.; De Feyter, S.; Hofkens, J.; Van der Auweraer, M.; De Schryver, F.; Brunner, K.; Hofstraat, J. W. Host Matrix Dependence on the Photophysical Properties of Individual Conjugated Polymer Chains. *Macromolecules* **2003**, *36*, 500–507.
10. Traiphol, R.; Sanguansat, P.; Srikhirin, T.; Kerdcharoen, T.; Osotchan, T. Spectroscopic Study of Photophysical Change in Collapsed Coils of Conjugated Polymers: Effects of Solvent and Temperature. *Macromolecules* **2006**, *39*, 1165–1172.
11. Ebihara, Y.; Vacha, M. Relating Conformation and Photophysics in Single MEH-PPV Chains. *J. Phys. Chem. B* **2008**, *112*, 12575–12578.
12. Liang, J.-J.; White, J.; Chen, Y.; Wang, C.; Hsiang, J.; Lim, T.; Sun, W.; Hsu, J.; Hsu, C.; Hayashi, M.; *et al*. Heterogeneous Energy Landscapes of Individual Luminescent Conjugated Polymers. *Phys. Rev. B* **2006**, *74*, 085209.
13. Ebihara, Y.; Habuchi, S.; Vacha, M. Conformation-Dependent Room-Temperature Emission Spectra of Single MEH-PPV Chains in Different Polymer Matrices. *Chem. Lett.* **2009**, *38*, 1094–1095.
14. Thompson, R. E.; Larson, D. R.; Webb, W. W. Precise Nanometer Localization Analysis for Individual Fluorescent Probes. *Biophys. J.* **2002**, *82*, 2775–2783.
15. Ahmet, Yildiz; Forkey, Joseph N.; McKinney, Sean A.; Ha, Taekjip; Goldman, Yale E.; Selvin, Paul R. Myosin V Walks Hand-Over-Hand: Single Fluorophore Imaging with 1.5-nm Localization. *Science* **2003**, *300*, 2061–2065.
16. Gordon, M. P.; Ha, T.; Selvin, P. R. Single-Molecule High-Resolution Imaging with Photobleaching. *Proc. Natl. Acad. Sci. U.S.A.* **2004**, *101*, 6462–6465.
17. Simonson, P. D.; Rothenberg, E.; Selvin, P. R. Single-Molecule-Based Super-Resolution Images in the Presence of Multiple Fluorophores. *Nano Lett.* **2011**, *11*, 5090–5096.
18. Habuchi, S.; Onda, S.; Vacha, M. Mapping the Emitting Sites within a Single Conjugated Polymer Molecule. *Chem. Commun.* **2009**, 4868–4870.
19. Habuchi, S.; Onda, S.; Vacha, M. Molecular Weight Dependence of Emission Intensity and Emitting Sites Distribution within Single Conjugated Polymer Molecules. *Phys. Chem. Chem. Phys.* **2011**, *13*, 1743–1753.
20. Wang, Y.; Fruhwirth, G.; Cai, E.; Ng, T.; Selvin, P. R. 3D Super-Resolution Imaging with Blinking Quantum Dots. *Nano Lett.* **2013**, *13*, 5233–5241.
21. Qu, X.; Wu, D.; Mets, L.; Scherer, N. F. Nanometer-Localized Multiple Single-Molecule Fluorescence Microscopy. *Proc. Natl. Acad. Sci. U.S.A.* **2004**, *101*, 11298–11303.
22. Burnette, D. T.; Sengupta, P.; Dai, Y.; Lippincott-Schwartz, J.; Kachar, B. Bleaching/blinking Assisted Localization Microscopy for Superresolution Imaging Using Standard Fluorescent Molecules. *Proc. Natl. Acad. Sci. U.S.A.* **2011**, *108*, 21081–21086.
23. Ober, R. J.; Ram, S.; Ward, E. S. Localization Accuracy in Single-Molecule Microscopy. *Biophys. J.* **2004**, *86*, 1185–1200.
24. Habuchi, S.; Oba, T.; Vacha, M. Multi-Beam Single-Molecule Defocused Fluorescence Imaging Reveals Local Anisotropic Nature of Polymer Thin Films. *Phys. Chem. Chem. Phys.* **2011**, *13*, 7001–7007.
25. Lin, H.; Hania, R. P.; Bloem, R.; Mirzov, O.; Thomsson, D.; Scheblykin, I. G. Single Chain *versus* Single Aggregate Spectroscopy of Conjugated Polymers. Where Is the Border? *Phys. Chem. Chem. Phys.* **2010**, *12*, 11770–11777.
26. Cheng K. Lee and Chi C. Hua. Nanomorphologies in Conjugated Polymer Solutions and Films for Application in Optoelectronics, Resolved by Multiscale Computation. In *Optoelectronics—Materials and Techniques*; Predeep, P., Ed.; In Tech: Croatia, 2011.
27. Hu, Dehong; Yu, Ji; Barbara, Paul F. Single-Molecule Spectroscopy of the Conjugated Polymer MEH-PPV. *J. Am. Chem. Soc.* **1999**, *121*, 6936–6937.
28. Teraoka, I. *Polymer Solutions: An Introduction to Physical Properties*; Wiley: New York, 2002.
29. Lee, C. K.; Hua, C. C.; Chen, S. A. Single-Chain and Aggregation Properties of Semiconducting Polymer Solutions Investigated by Coarse-Grained Langevin Dynamics Simulation. *J. Phys. Chem. B* **2008**, *112*, 11479–11489.
30. Bhattacharjee, S. M.; Giacometti, A.; Maritan, A. Flory Theory for Polymers. *J. Phys.: Condens. Matter* **2013**, *25*, 503101.
31. Rothberg, L. Conjugated Polymers: Watching Polymers Dance. *Nat. Chem.* **2011**, *3*, 425–426.
32. Mirzov, O.; Cichos, F.; von Borczyskowski, C.; Scheblykin, I. Direct Exciton Quenching in Single Molecules of MEH-PPV at 77 K. *Chem. Phys. Lett.* **2004**, *386*, 286–290.
33. Neef, C. J.; Ferraris, J. P. MEH-PPV: Improved Synthetic Procedure and Molecular Weight Control. *Macromolecules* **2000**, *33*, 2311–2314.